Department of Mathematics and Statistics

Preprint MPCS-2019-01

11 March 2019

the number of DOFs needed to achieve a given accuracy (for scattering by a convex polygon in two-dimensions) was shown to depend only logarithmically on the frequency for the h-BEM version of HNA in Chandler-Wilde & Langdon (2007), this improved to the hp-BEM version in Hewett *et al.* (2013). These ideas were extended, in Chandler-Wilde *et al.* (2015), to a certain class of non-convex polygons, with the high frequency asymptotics arising from re-reflections and partial illumination (shadowing) being fully captured by a careful choice of approximation space. Similar ideas have been applied to penetrable obstacles in Groth *et al.* (2015, 2018) and to two- and three-dimensional screens in Hewett *et al.* (2015) and Hargreaves *et al.* (2015) respectively. All of these methods are, broadly speaking, for single obstacles and for plane wave incidence (although an extension to other incident fields is discussed

determine the total field $u \quad C^2(D) \cap C(\bar{D})$ such that

$$\Delta u + k^2 u = 0 \qquad \text{in } D, \tag{2.2}$$

$$u = 0 \qquad \text{on} \quad D = \quad \cup \tag{2.3}$$

and u

Naturally, one can rotate the coordinate system if required to ensure the above conditions hold. The (R_0,R_1) condition is central to many of the estimates in this paper, as this is the regime in which k-explicit estimates for Dirichlet-to-Neumann maps are currently known. From these we can obtain estimates of the solution to the boundary integral equation defined below. For further explanation and examples of (R_0,R_1) configurations, we refer to Chandler-Wilde *et al.* (2018, § 1.2.1).

The BVP (2.2)–(2.4) can be reformulated as a boundary integral equation (BIE). We denote the single layer potential $S_k : L^2(\partial D) \to C^2(D)$ by

$$S_k\varphi(\mathbf{x}) := \int_{\partial D} \Phi_k(\mathbf{x},\mathbf{y})\varphi(\mathbf{y})\,\mathrm{d}s(\mathbf{y}), \quad \mathbf{x} \in D, \tag{2.5}$$

where $\Phi_k(\mathbf{x},\mathbf{y}) := (\mathrm{i}/4)H_0^{(1)}(k|\mathbf{x}-\mathbf{y}|)$ is the fundamental solution of (2.2), in which $H_0^{(1)}$ denotes the Hankel function of the first kind and order zero. If u satisfies the BVP (2.2)–(2.4), then $\partial u/\partial\mathbf{n} \in L^2(\partial D)$ and the following Green's representation holds (see, e.g., Chandler-Wilde *et al.* (2012, Theorem 2.43))

$$u = u^i - S_k\frac{\partial u}{\partial \mathbf{n}} \quad \text{in } D. \tag{2.6}$$

DEFINITION 2.4 (Combined potential operator) The standard combined potential operator $\mathsf{A}_{k,\eta} : L^2(\partial D) \to L^2(\partial D)$ (see, e.g., Colton & Kress (2013); Chandler-Wilde *et al.* (2012)) is defined by

$$\mathsf{A}_{k,\eta} := \frac{1}{2}\mathsf{I} + \mathsf{D}_k' - \mathrm{i}\eta\mathsf{S}_k,$$

where I is the identity operator, $\eta \in \mathbb{R}\setminus\{0\}$ is a coupling parameter,

$$\mathsf{S}_k\varphi(\mathbf{x}) := \int_{\partial D} \Phi_k(\mathbf{x},\mathbf{y})\varphi(\mathbf{y})\,\mathrm{d}s(\mathbf{y}), \quad \mathbf{x} \in \partial D, \quad \varphi \in L^2(\partial D),$$

denotes the single layer operator and

$$\mathsf{D}_k'\varphi(\mathbf{x}) := \int_{\partial D} \frac{\partial\Phi_k(\mathbf{x},\mathbf{y})}{\partial\mathbf{n}(\mathbf{x})}\varphi(\mathbf{y})\,\mathrm{d}s(\mathbf{y}), \quad \mathbf{x} \in \partial D, \quad \varphi \in L^2(\partial D),$$

denotes the adjoint of the double-layer operator.

From (2.6), the BVP (2.2)–(2.3) can be reformulated as a BIE (Chandler-Wilde *et al.*, 2012, (2.69), (2.114))

$$\mathsf{A}_{k,\eta}\frac{\partial u}{\partial \mathbf{n}} = f_{k,\eta}, \quad \text{on } \partial D, \tag{2.7}$$

where the right-hand side data $f_{k,\eta} \in L^2(\partial D)$ is

$$f_{k,\eta} = \left(\frac{\partial}{\partial\mathbf{n}} - \mathrm{i}\eta\right)u^i. \tag{2.8}$$

It follows from Chandler-Wilde *et al.* (2012, Theorem 2.27) that $\mathsf{A}_{k,\eta}$ is invertible. We shall solve the BIE (2.7) numerically using an oscillatory basis, the use of which is justified by the representation and regularity results in the next section.

3. Representation and regularity of solution on

The structure of this section is as follows: In

$$= \int_{\ U_j} \left[\frac{G_j(\mathbf{x},\mathbf{y})}{\mathbf{n}\ (\mathbf{y})} \big(\underbrace{u(\mathbf{y})\ \ u^i(\mathbf{y})}_{=0} \big)\ \ G_j(\mathbf{x},\mathbf{y}) \frac{(u\ \ u^i)(\mathbf{y})}{\mathbf{n}} \right] \mathrm{d}s(\mathbf{y})$$

$$\overset{(3.4)}{=} \int_{\ U_j} G_j(\mathbf{x},\mathbf{y}) \frac{u(\mathbf{y})}{\mathbf{n}} \mathrm{d}s(\mathbf{y}) + \int_{j\ } \left[\frac{G_j(\mathbf{x},\mathbf{y})}{\mathbf{n}_j(\mathbf{y})} u^i(\mathbf{y}) + G_j(\mathbf{x},\mathbf{y}) \frac{u^i(\mathbf{y})}{\mathbf{n}} \right] \mathrm{d}s(\mathbf{y}).$$

Substituting this expression in (3.3) and using again (3.1), we obtain a representation for u^s:

$$u^s(\mathbf{x}) = 2 \int_{j} \frac{{}_k(\mathbf{x},\mathbf{y})}{\mathbf{n}_j(\mathbf{y})} u^s(\mathbf{y})\, \mathrm{d}s(\mathbf{y})\ \int_{\ U_j} G_j(\mathbf{x},\mathbf{y}) \frac{u(\mathbf{y})}{\mathbf{n}} \mathrm{d}s(\mathbf{y})$$

$$2 \int_{j\ } \frac{{}_k(\mathbf{x},\mathbf{y})}{\mathbf{n}_j(\mathbf{y})} u^i(\mathbf{y})\, \mathrm{d}s(\mathbf{y}), \qquad \mathbf{x} \quad D\ \ U_j. \tag{3.5}$$

)

Summing with (3.5) and taking the Neumann trace gives the representation for $u/\ \mathbf{n}$ on $_j$:

$$\frac{u(\mathbf{x})}{\mathbf{n}} = 2\frac{u^i(\mathbf{x})}{\mathbf{n}} + 2\int_{j} \frac{^2\ {}_k(\mathbf{x},\mathbf{y})}{\mathbf{n}_j(\mathbf{x})\ \ \mathbf{n}_j(\mathbf{y})} u(\mathbf{y})\,\mathrm{d}s(\mathbf{y})$$
$$-\ 2\int_{U_j} \frac{{}_k(\mathbf{x},\mathbf{y})}{\mathbf{n}_j(\mathbf{x})}\frac{u(\mathbf{y})}{\mathbf{n}}\,\mathrm{d}s(\mathbf{y}), \qquad \mathbf{x}\ \ _j, \quad \mathbf{n}_j\ \ \mathbf{d}<0, \tag{3.7}$$

where we used again (3.1) and $u^r/\ \mathbf{n}_j = \ u^i/\ \mathbf{n}_j$ on $_j$.

The representation (3.6)–(3.7) may be viewed as a correction to the Physical Optics approximation for a single scatterer, which is defined as

$$(\mathbf{x}) := \begin{cases} 2\ \ u^i(\mathbf{x})/\ \ \mathbf{n}, & \mathbf{x}\ \ \ _j \quad :\mathbf{n}_j(\mathbf{x})\ \ \mathbf{d}<0, \\ 0, & \mathbf{x}\ \ \ _j \quad :\mathbf{n}_j(\mathbf{x})\ \ \mathbf{d}\geqslant 0. \end{cases} \tag{3.8}$$

Specifically, this correction can be split into two parts. The first integral of (3.6) and (3.7) represents the waves diffracted by the corners of (diffraction is ignored by the Physical Optics approximation), whilst the second integral represents the correction to the waves reflected by the sides of , as a result of the presence of . Unless the distance between the scatterers is sufficiently large, it is reasonable to expect the second correcting term to be not negligible.

We now write more explicitly the integral representation (3.6)–(3.7) in terms of the parametrisations of the segments $_j$ and of their extensions $_j$. From the standard properties of Bessel functions (see, e.g., DLMF (2019, 10)), we have that for $\mathbf{x}\ \ _j$, $\mathbf{y}\ \ _j$,

$$\frac{^2\ {}_k(\mathbf{x},\mathbf{y})}{\mathbf{n}(\mathbf{x})}$$

we shall now discuss each term in the ansatz separately. Here is the Physical Optics approximation (3.8), with the envelopes of the diffracted waves on each side defined by

$$v_j^{+}(s) := \frac{\mathrm{i}k^2}{2}\int_{(0,\ )\ Z_j^{+}} \big(k(s+t)\big)\mathrm{e}^{\mathrm{i}k(t\ \ \widetilde{L}_{j}\ \ 1)}u\big(\mathbf{y}_j(\widetilde{L}_{j}\ \ 1\ \ t)\big)\,\mathrm{d}t,\ s\ \ [0,L_j], \tag{3.11}$$

$$v_j(s) := \frac{\mathrm{i}k^2}{2}\int_{(0,\ )\ Z_j} \big(k(s+t)\big)\mathrm{e}^{\mathrm{i}k(\widetilde{L}_j+t)}u\big(\mathbf{y}_j(\widetilde{L}_j+t)\big)\,\mathrm{d}t,\ s\ \ [0,L_j], \tag{3.12}$$

where $Z_j^{+} := \ t\ \ \mathbb{R} : \mathbf{y}_j(\widetilde{L}_{j}\ \ 1\ \ t)$ and $Z_j := \ t\ \ \mathbb{R} : \mathbf{y}_j(\widetilde{L}_j+t)$ are used to exclude from the integral the points inside (as is the case for $_3$ of Figure 2), to remain consistent with (3.6)–(3.7). The *interaction operator* $\mathsf{G}_{\to\ \ j} : L^2(\ )\ \ L^2(\ _j)$ used in (3.10) is based on the final term of (3.6)–(3.7), and is defined by

$$\mathsf{G}_{\to\ \ j}\ (\mathbf{x}) := 2\int_{\ U_j} \frac{_k(\mathbf{x},\mathbf{y})}{\mathbf{n}_j(\mathbf{x})}\ (\mathbf{y})\,\mathrm{d}s(\mathbf{y}),\quad \mathbf{x}\ \ \ _j\ \ , \tag{3.13}$$

for $L^2(\ )$. We extend this definition to $\mathsf{G}_{\to} : L^2(\ )\ \ L^2(\ )$ as

$$\mathsf{G}_{\to}\ := \mathsf{G}_{\to\ \ j}\ \text{ on }\ _j\ \text{ for } j = 1,\ldots,\mathsf{N}\ ,\text{ and }\ L^2(\ ). \tag{3.14}$$

REMARK 3.1 The ansatz (3.10) is an extension of Chandler-Wilde & Langdon (2007, (3.9)) and Hewett *et al.* (2013, (3.2)), with an additional term which relates the solution on to the solution on . It is important to note that this additional term is not the only term influenced by the presence of and that one cannot solve for v on a single scatterer and then add the $\mathsf{G}_{\to}\ [\ u/\ \mathbf{n}\ ]$ term. The reason for this is clear from (3.11)–(3.12): even if Z_j were of measure zero, so that the equations for (3.11)–(3.12) were identical to the case of a single scatterer, the integral contains u, which depends on the configuration D. Intuitively this makes sense, diffracted waves emanating from the corners of will also be influenced by the presence of additional scatterers.

Many of the bounds which follow are explicit only in k or the parameters which determine mesh-width or polynomial degree of an approximation space. Henceforth we will use $A \lesssim B$ to mean $A \leqslant CB$, where C is a constant that depends only on the geometry of . To gauge the size of the contribution to the reflected waves on arising from the presence of , we require the following bound on the operator $\mathsf{G}_{\to}$.

LEMMA 3.1 For $D = \ \cup\ $ with and disjoint, we have the following bound on the interaction operator $\mathsf{G}_{\to}$ defined in (3.14), given $k_0 > 0$:

$$\|\mathsf{G}_{\to}\|_{L^2(\ )\to L^2(\ )} \leqslant C_{\mathsf{G}}(k) \lesssim \sqrt{k},\quad \text{for } k \geqslant k_0,$$

where

$$C_{\mathsf{G}}(k) := \sqrt{\frac{L\ \ L\ \ k}{2\pi\,\mathrm{dist}(\ ,\ )}} + \frac{\sqrt{L\ \ L\ }}{\pi\,\mathrm{dist}(\ ,\ )}, \tag{3.15}$$

where L and L denote the perimeters of and respectively.

Proof. For $0 \neq \ \ L^2(\ )$, using the Cauchy–Schwarz inequality, we can write

$$\leqslant \frac{2}{L^2(\ )} \left(\int \left\| \frac{_k(\mathbf{x},\ )}{\mathbf{n}(\mathbf{x})} \right\|^2_{L^2(\ )} \ {}^{2}_{L^2(\ )} \, \mathrm{d}s(\mathbf{x}) \right)^{1/2}$$

$$= 2 \left(\int \int \left| \frac{_k(\mathbf{x},\mathbf{y})}{\mathbf{n}(\mathbf{x})} \right|^2 \mathrm{d}s(\mathbf{y}) \, \mathrm{d}s(\mathbf{x}) \right)^{1/2}$$

$$\leqslant 2 \left(\int \mathrm{d}s \int \mathrm{d}s \right)^{1/2} \sup_{\mathbf{x} \quad ,\mathbf{y}} \left| \frac{_k(\mathbf{x},\mathbf{y})}{\mathbf{n}(\mathbf{x})} \right|.$$

The result follows from $H_0^{(1)}\ (z) = \ H_1^{(1)}(z)$ and Chandler-Wilde *et al.*

case (i), the integral is bounded above by

$$\hat{c}^2 \int_1^{1+kR_D} s^{-1}\,\mathrm{d}s = \hat{c}^2 \log(1+kR_D)$$

and in case (ii) it is bounded above by

$$2\hat{c}^2 \int_1^{kR_D/2} s^{-1}\,\mathrm{d}s = 2\hat{c}^2 \log(kR_D/2),$$

so in either case, (3.20) is bounded above by $2\hat{c}^2\log(1+kR_D)$. Combining this with (3.21) yields

$$\|\psi_k(\mathbf{p},\cdot)\|^2_{L^2(\Gamma_D)} \leqslant \frac{1}{k} N_D \hat{c}^2 \frac{\sqrt{1+C_\ell^2}}{8}\Big(5+\log(1+kR_D)\Big),$$

This gives the explicit form of the simplified estimate in our claim, proving the assertion. □

Using this result, we can say more about the k-dependence of 12S992 0 Td518755964(u)-5.883 4.684 Tf d [5.51992 0

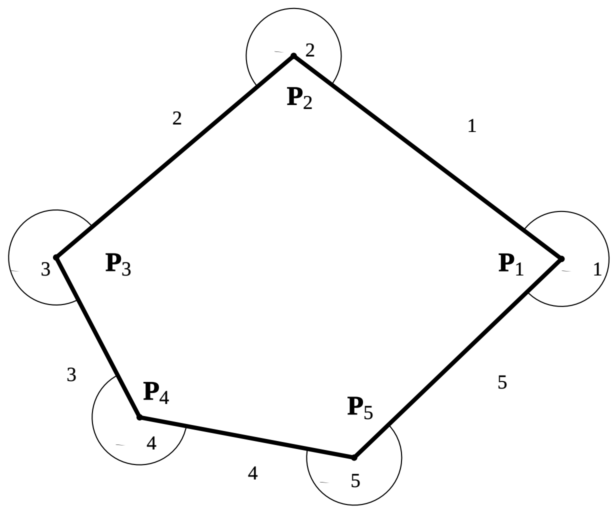

FIG. 3: A convex polygon with the parameters introduced in 3.3.

LEMMA 3.3 (Solution behaviour near the corners) Suppose that u satisfies the BVP (2.2)–(2.4) and $\mathbf{x}$ D satisfies $r := \mathbf{x}\ \ \mathbf{P}_j\ \ (0,1/k]$, and $r < \mathrm{dist}(\mathbf{P}_j,\ )$. Then there exists a constant $C > 0$, depending only on D and c_*, such that (with $u_{\max}(k)$ as in (3.16)),

$$u(\mathbf{x}) \leqslant C(kr)^{\pi/\ \ j} u_{\max}(k).$$

Proof. Follows identical arguments to Hewett *et al.* (2013, Lemma 3.5), with the slight modification to the definition $R_j := \min\ L$

4. hp approximation space

We will combine two approximation spaces: the HNA-BEM space on and a standard hp-BEM space on . Hereafter, using the parametrisation of the boundaries and , we identify $L^2(\ _j)$ with $L^2(0,L_j)$, and $L^2(\ )$ with $L^2(0,L\ )$.

4.1 *HNA-BEM approximation on*

As in previous HNA methods, on we approximate only the diffracted waves

$$v\ (s) := \frac{1}{k}\left(v_j^{+}(s\ \ \widetilde{L}_{j\ \ 1})\mathrm{e}^{\mathrm{i}ks} + v_j\ (\widetilde{L}_j\ \ s)\mathrm{e}^{\ \ \mathrm{i}ks}\right), \quad s$$

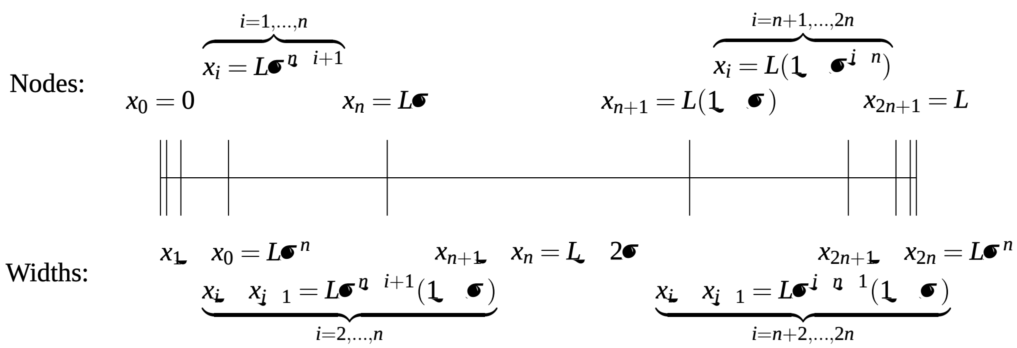

FIG. 4: The single-mesh space of Definition 4.1 on a segment $[0,L]$.

DEFINITION 4.1 Given $L>0$, $n\in\mathbb{N}$ and a grading parameter $\sigma\in(0,1/2)$, we denote by $\mathbf{M}_n(0,L) = \{x_0,\dots,x_{2n+1}\}$ the symmetric geometrically where

$$x_{\tilde{n}_j} := \max\left\{x_i \quad \mathbf{M}_{n_j}(0,L_j) \text{ such that } x_i \leqslant \quad {}_j\frac{2\pi}{k}\right\}$$

Theorem 4.2 shows that we obtain exponential convergence of the best approximation to $v_{\setminus}$ with respect to p , which controls both polynomial degree and mesh grading (via (4.2)), across all wavenumbers k. To maintain accuracy as k increases one needs to increase p in proportion to $\log k$, and hence the total number of degrees of freedom (which is proportional to p^2) in proportion to $\log^2 k$.

REMARK 4.2 It is shown in Hewett *et al.* (2011, Theorem A.3) for the overlapping-mesh HNA space that it is possible to reduce the number of degrees of freedom on , whilst maintaining exponential convergence, by reducing the polynomial degree in the smaller mesh elements, as is standard in *hp* schemes. For example, given a polynomial degree $p_j > 1$, we can define for each side $_j$, $j = 1, \ldots, \mathbf{N}$, a degree vector $\mathbf{p}_j$ by

$$(\mathbf{p}_j)_i := \begin{cases} p_j \quad \left\lfloor \frac{n_j+1 \quad i}{n_j} p_j \right\rfloor, & 1 \leqslant i \leqslant n_j, \\ p_j, & i = n_j + 1, \end{cases}$$

where n_j is as in Definition 4.1 of the single-mesh space. This may be applied to either the single or overlapping mesh, and results in a linear reduction of polynomial degree on mesh elements closer to the corners of $_j$. Numerical experiments in 6 suggest that exponential convergence is maintained for the single-mesh HNA space if the degrees of freedom are reduced in this way, although we do not prove this here.

4.2 *Standard hp-BEM approximation on*

If Assumption 3.2 holds, as is the case in the configurations of Theorem 3.1, it follows from Theorem 4.2 that it is sufficient for the number of DOFs in $V_N^{\mathrm{HNA}}(\;)$ to grow logarithmically with k, to accurately approximate $v_{\setminus}$. However, this tells us nothing about the DOFs required on . To account for the contribution from , we parametrise $\mathbf{x}$: $[0, L\;]$ and construct an appropriate (depending on the geometry of) N -dimensional approximation space $V_N^{hp}(\;) \quad L^2(0, L\;)$ for

$$v\;(s) := \frac{1}{k} \frac{u}{\mathbf{n}} \big(\mathbf{x}\;(s)\big), \quad s \quad [0, L\;]. \tag{4.3}$$

While a representation analogous to (3.10) holds on when is a convex polygon, this approach is not suitable for the present multiple scattering approximation. If such a representation were used on multiple polygons, the system to solve would need to be written as a Neumann series and solved iteratively. This alternative approach is outlined b5.89115(n)-5.8887(s)3.71(t)0.965521(hh7R109.96264Tf3.839840Td[(0)-5.8887]TJ/R389.96264a)-

configurations (of Definition 2.3) for which we have from Chandler-Wilde *et al.* (2018, (1.28)): if $= O(k)$, then given $k_0 > 0$,

$$\mathbf{A}_{k,}^{1} \quad L^{2}($$

Proof. Throughout the proof we let C denote an arbitrary constant independent of k and n. It follows from standard mapping properties of the single-layer operator (e.g., Chandler-Wilde *et al.* (2012, Theorem 2.15(i))) that $u^i \quad H^1(\quad)$, where is a bounded open subset of $\mathbb{R}^2$ containing $\cup$. We may therefore bound using Melenk (2012, Theorem B.6), choosing zero forcing term to obtain

$$u^i \quad _{H^{n+2}(T\ )} \leqslant Ck^{n+2} \quad u^i \quad _{L^2(\quad)}, \quad \text{for } k \geqslant k_0, \quad n \quad \mathbb{N}_0, \tag{4.8}$$

given $k_0 > 0$, where is a bounded open set compactly containing T and . From (4.7), we see that the norm is the sum of $n+1$ terms, hence

$$\begin{aligned} \nabla^n u^i \quad ^2_{L^2(T\ )} &\leqslant (n+1)! \quad u^i \quad ^2_{H^{n+2}(T\ )}, \qquad (4.9)\\ &\leqslant C(n+1)^n k^{n+2} \quad u^i \quad ^2_{L^2(\quad)}, \quad \text{for } k \geqslant k_0, \quad n \quad \mathbb{N}_0, \qquad (4.10) \end{aligned}$$

given $k_0 > 0$, which follows by combining with (4.8) and $(n+1)! \leqslant (n+1)^n$. We now bound u^i in terms of known quantities,

$$u^i \quad _{L^2(\quad)} \leqslant \quad ^{1/2} \quad S_k \quad _{L^2(\quad) \to L\ (\quad)} \quad \mathsf{A}_{\bar{k},}^{\ 1} \quad _{L^2(\quad) \to L^2(\quad)} \quad f_{k,} \quad _{L^2(\quad)}.$$

We may bound these norms using Lemma 3.17, (4.4) and (2.8) (choosing $\quad = O(k)$) to obtain

$$u^i \quad _{L^2(\quad)} \leqslant Ck^{5/2} \log^{1/2}(k\,\mathrm{diam}(\quad) + 1). \tag{4.11}$$

Finally, we can combine the bound (4.11) with (4.10) to obtain

$$\nabla^n u^i \quad _{L^2(T\ )} \leqslant Ck^{7/2} \log^{1/2}(k\,\mathrm{diam}(\quad) + 1)$$

DEFINITION

and

$$\mathbf{b} := \frac{1}{k}\left[\frac{(f \quad \mathsf{A} \rightarrow \quad , \phi)_{L^2(\ )}}{(f \quad \mathsf{A} \rightarrow \quad , \phi)_{L^2(\ )}}\right] \begin{matrix} \phi \quad \Lambda \\ \phi \quad \Lambda \end{matrix}$$

(v) p , C and τ are as in Assumption 4.4.

Proof. First we focus on the best approximation of $u/$ **n** by an element $w = (w \;, w \;)$ of $V_N^{\mathrm{HNA}^*}(\;,\;)$. By the definition (4.13) we have

$$\inf_{w \quad V_N^{\mathrm{HNA}^*}(\;,\;)} \left(\left\| \frac{u}{\mathbf{n}} \quad (\quad + kw \quad + k\mathbf{G}_{\rightarrow} \; w \;) \right\|_{L^2(\;)} + \left\| \frac{u}{\mathbf{n}} \quad kw \quad \right\|_{L^2(\;)} \right)$$

$$= k \inf_{w \quad V_N^{\mathrm{HNA}^*}(\;,\;)} \left(\left\| [v \quad w \quad] + \mathbf{G}_{\rightarrow} \; [v \quad w \quad] \right\|^2_{L^2(\;)} + \| v \quad w$$

$$k\int_0^{L} \left(\mathbf{x},\mathbf{y}\ (s)\right) v^{N}\ (s)\,\mathrm{d}s, \qquad \text{for } \mathbf{x}\quad D. \tag{5.10}$$

Here the parametrisation $\mathbf{y}$ is as in (3.9) and $\mathbf{y}$ as in 4.2. Expanding further, we can extend the definition of $\mathbf{G}_{\rightarrow}$ to a parametrised form by

$$\left(\mathbf{G}_{\rightarrow}\ v^{N}\right)(s) := \int_0^{L} \ (s,t) \frac{k(\mathbf{y}\ (s),\mathbf{y}\ (t))}{\mathbf{n}(\mathbf{y}\ (s))} v^{N}\ (t)\,\mathrm{d}t, \quad s \quad [0,L\ ],$$

where the indicator function

$$(s,t) := \begin{cases} 1, & \mathbf{y}\ (s) \quad {}_j \text{ and } \mathbf{y}\ (t) \quad U_j, \\ 0, & \text{otherwise}, \end{cases}$$

is used to ensure the path of integration remains inside the relative upper half-plane U_j.

COROLLARY 5.1 Assume conditions *(i)–(iv)* of Theorem 5.1 hold. Then given $k_0 > 0$, the HNA-BEM approximation to the BVP (2.2)–(2.4) satisfies the error bound

$$u \quad u_{N\ L\ (D)} \lesssim C_q(k) k^{1/2} \log^{1/2}(1 + k\,\mathrm{diam}(\ D))$$
$$\Big(C_u C\ \ k$$

COROLLARY 5.2 Under the assumption of Theorem 5.1, the far-field pattern u_N computed from the HNA-BEM solution approximates u with the error bound

$$\|u - u_N\|_{L (0,2\pi)} \leqslant C_q(k)k\sqrt{L + L} \left(C_u C \, k^{- 1/2} J(k) e^{\tau p} + [1 + C(k)] C (k) e^{\tau (k) p} \right).$$

The terms in the bound are as in Theorem 5.1.

Proof. We have

$$u ( ) - u_N( ) \leqslant \int_{D} \left| \frac{u}{\mathbf{n}} - N \right| \mathrm{d}s \leqslant (L + L)^{1/2} \left\| \frac{u}{\mathbf{n}} - N \right\|_{L^2(D)}$$

and the result follows by Theorem 5.1. □

6. Numerical results

Here we present numerical results for the solution of the discrete problem (5.2)–(5.3). The configuration tested consists of two equilateral triangles with perimeters $L = 6\pi$ and $L = 3\pi/5$, separated by dist(,) = $\sqrt{3}\pi/5$, as in Figure 5. It follows that there are exactly k wavelengths on each side of and $k/10$ on each side of . Experiments were run for k 20, 40, 80, 160 (so the number of wavelengths across the perimeter D ranges from 66 to 528) and a range of incident directions $\mathbf{d}$, for $p = p = p$ 1, ..., 8 . In terms of observed error, each value of $\mathbf{d}$ tested gave very similar results, hence we focus here on the case $\mathbf{d} = (1,1)/\sqrt{2}$, which allows some re-reflections between the obstacles and partial illumination of , see Figure 5.

To construct the approximation space $V_N^{\mathrm{HNA}^*}(,)$, we first choose $V_N^{\mathrm{HNA}}( )$ to be the single-mesh approximation space of 4 with $p_j = p$ for each side $j = 1, \ldots, \mathbf{N} = 3$, reducing the polynomial degree close to the corners of in accordance with Remark 4.2, hence p now refers to the polynomial degree on the largest mesh elements. We also remove basis elements close to the corners of the mesh on in accordance with Remark 4.1, choosing $j = \max (1 + p)/4, 2$, to improve conditioning of the discrete system (5.4). A grading parameter of $= 0.15$ is used (as in Hewett *et al.* (2011), where the rationale for this choice is discussed), with $n_j = 2p$ layers on each graded mesh, for $j = 1, 2, 3$ (hence we may choose the constant from Theorem 4.2 as $c_j = 2$).

Theorem 4.2 ensures that we will observe exponential convergence on if the polynomial degree is consistent across the mesh, and Proposition 4.3 ensures that we observe exponential convergence on if is analytic. In these numerical experiments we test problems where these two conditions are not met, and encouragingly still observe exponential convergence. As hypothesised by Remark 4.2 and Assumption 4.4, our experiments suggest that our method converges exponentially under conditions much broader than those guaranteed by our theory.

For the standard hp-BEM space $V_N^{hp}( )$, we use the same parameters p_j, and c_j to grade towards the corners of , so the construction of the mesh on is much the same as on . The key difference is that on every mesh element is sufficiently subdivided to resolve the oscillations. The polynomial degree p_j is decreased on smaller elements, as on , in accordance with Remark 4.1.

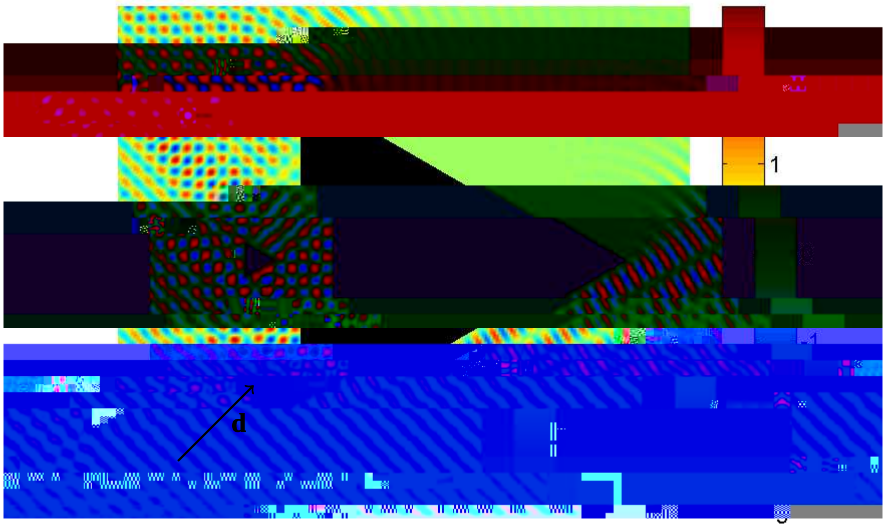

FIG. 5: The total field Re u_N for scattering by two triangles, at the lowest frequency considered. Here $L = 6\pi$, $L = 3\pi/5$, $k = 20$, $\mathbf{d} = (1,1)/$

REMARK 6.1 (Quadrature) The integrals in (5.4) and (5.5) and the L^2 norms used to estimate the error in Figure 7 may be oscillatory and singular. In particular, care must be taken when evaluating the triple integral $\big(\mathbf{A} \; _{\rightarrow} \; \mathbf{G} \; _{\rightarrow} \; v,$

BETCKE, T., CHANDLER-WILDE, S. N., GRAHAM, I. G., LANGDON, S. & LINDNER., M. (2011) Condition number estimates for combined potential boundary integral operators in acoustics and their boundary element discretisation. *Numer. Methods PDEs*, **27**, 31–69.

BONNET, M., COLLINO, F., DEMALDENT, E., IMPERIALE, A. & PESUDO, L. (2018) A hybrid method combining the surface integral equation method and ray tracing for the numerical simulation of high frequency diffraction involved in ultrasonic NDT. *J. Phys. Conf. Ser.*, **1017**, 012007.

BOUBENDIR, Y., ECEVIT, F. & REITICH, F. (2017) Acceleration of an iterative method for the evaluation of high-frequency multiple scattering effects. *SIAM J. Sci. Comput.*, **39**, B1130–B1155.

CHANDLER-W

GIBBS, A. (2017) Numerical methods for high frequency scattering by multiple obstacles. *Ph.D. thesis*, University of Reading. http://centaur.reading.ac.uk/73458/.

GIBBS, A., HEWETT, D., HUYBRECHS, D. & PAROLIN, E. (2019) Fast hybrid numerical-asymptotic boundary element methods for high frequency screen and aper

SPENCE, E. A., CHANDLER-WILDE, S. N., GRAHAM, I. G. & SMYSHLYAEV, V. P. (2011) A new frequency-uniform coercive boundary integral equation for acoustic scattering. *Comm. Pure Appl. Math.*, **64**, 1384–1415.

SPENCE, E. A. (2014) Wavenumber-explicit bounds in time-harmonic acoustic scattering. *SIAM J. Math. Anal.*, **46**, 2987–3024.

A. A coercive multiple scattering formulation

In § 5 it was noted that there exists a boundary integral formulation of the BVP (2.2)–(2.4) which is *coercive* (sometimes called V-elliptic), provided is of the order of one wavelength. With a coercive formulation, it follows by the Lax–Milgram Theorem that the corresponding discrete problem (equivalent to (5.4)–(5.5)) is well posed, on any finite dimensional subspace of $L^2(\ \cup \ )$. We now present this formulation.

For problems of scattering by a single star-shaped obstacle, it was shown in Spence *et al.* (2011) that the *star combined* formulation is coercive for problems on a single star-shaped obstacle. In the thesis Gibbs (2017) this formulation was extended to the *constellation combined* formulation, where it was shown to be coercive for certain configurations consisting of multiple star-shaped obstacles. We present a version with sharper bounds here, specialising the coercivity result to the case of one large obstacle and one or many small obstacles . We begin by formally defining the configurations of interest:

DEFINITION A.1 (Star- and constellation-shaped) A bounded open set with boundary is *star-shaped* if there exists $\mathbf{x}^c$ and a Lipschitz continuous $g : S^1 \quad \mathbb{R}$, where $S^1 := \{ \hat{\mathbf{x}} \quad \mathbb{R}^2 : |\hat{\mathbf{x}}| = 1 \}$, such that $g(\hat{\mathbf{x}}) > 0$ for all $\hat{\mathbf{x}} \quad S^1$ with

$$ = \{ \mathbf{x}^c + g(\hat{\mathbf{x}})(\hat{\mathbf{x}} \quad \mathbf{x}^c) : \hat{\mathbf{x}} \quad S^1 \} .$$

Intuitively, this may be interpreted as the following: Given any $\mathbf{x}$, one can draw a straight line from $\mathbf{x}^c$ to $\mathbf{x}$, without leaving .

We say a domain is *constellation-shaped* if it can be represented as the finite union of multiple star-shaped, pairwise disjoint obstacles. In such a case, for each star-shaped component we denote the above $\mathbf{x}^c$ parameter by $\mathbf{x}_i^c$, where i is the index of that component.

We will use the integral operator

$$\nabla_S \mathbf{S}_k \quad (\mathbf{x}) := \int \nabla_S \quad {}_k(\mathbf{x},\mathbf{y}) \quad (\mathbf{y})\,\mathrm{d}s(\mathbf{y}), \quad \text{for} \quad L^2(\quad), \quad \mathbf{x} \quad , \tag{A.1}$$

with the surface gradient operator of the fundamental solution as its kernel:

$$\nabla_S \quad {}_k(\mathbf{x},\mathbf{y}) := \nabla \quad {}_k(\mathbf{x},\mathbf{y}) \quad \mathbf{n}(\mathbf{x}) \frac{{}_k(\mathbf{x},\mathbf{y})}{\mathbf{n}(\mathbf{x})}, \tag{A.2}$$

where

where $\mathbf{Z}(\mathbf{x}) = \mathbf{x} \quad \mathbf{x}_i^c$ (with $\mathbf{x}_i^c \quad {}_i$ chosen as $\mathbf{x}^c$ for each star-shaped component in Definition A.1) on ${}_i$, for $i = 1, \ldots, N$ and $\hat{}\,(\mathbf{x}) := k\,\mathbf{Z}(\mathbf{x}) \; + \mathrm{i}/2$. This operator yields an alternative BIE to (2.7), namely

$$\mathsf{A}_k \frac{u}{\mathbf{n}} = f_k, \quad \text{on} \quad ,$$

where the right-hand side data is

$$f_k := (\mathbf{Z} \;\nabla \quad \mathrm{i}\,\hat{}\,)\,u^i, \quad \text{on} \quad .$$

Invertibility of A_k follows by Chandler-Wilde *et al.*

$$\leqslant \left(k\,\mathrm{diam}(X)+\frac{1}{2}\right)\left[\sqrt{\frac{1}{2\pi k\,\mathrm{dist}(X,Y)}}+\frac{1}{2\pi k\,\mathrm{dist}(X,Y)}\right].$$

We want to find conditions under which the right-hand side of the above inequality is positive, hence we require the negative term to be sufficiently small. We bound these off-diagonal terms

$$\left|(\mathbf{A}_{\text{cross}}\ \ ,\ \ )_{L^2(\ \cup\ )}\right| \leqslant \ \mathbf{A}_{\text{cross}}\ \ _{L^2(\ \cup\ )\to L^2(\ \cup\ )}\ \ \ \ ^{2}_{L^2(\ \cup\ )}. \tag{A.9}$$

We now split the above norm on $\mathbf{A}_{\text{cross}}$ using the triangle inequality noting the terms in (A.6), and apply the bound (A.4) to each component,

$$\mathbf{A}_{\text{cross}}\ \ _{L^2(\ \cup\ )\to L^2(\ \cup\ )} \leqslant \ \mathbf{A}_{k,\ \ \to}\ \ + \ \mathbf{A}_{k,\ \ \to}\ \ + \sum_{i=1}^{\mathbf{N}} \ \mathbf{A}_{k,\ \ i\to(\ \ i)}$$

$$\leqslant^{1}$$

Proof.